Impedance spectra of hot, dry silicate minerals and rock: Qualitative interpretation of spectra

J. Stephen Huebner, Roberta G. Dillenburg

U.S. Geological Survey, Reston, Virginia 22092, U.S.A.

Abstract

Impedance spectroscopy helps distinguish the contributions that grain interiors and grain boundaries make to electrical resistance of silicate minerals and rocks. The technique also distinguishes the low-frequency response due to the presence of instrument electrodes. We measured olivine, orthopyroxene, clinopyroxenes, and both natural and synthetic clinopyroxenite. Measurements were made at 1 bar, from 750 to 1150 °C, and over a frequency range from $<10^{-4}$ to $>10^6$ Hz; some measurements were also made at 300–850 °C and 10–20 kbar. The grain-interior response lies at highest frequency, the sample-electrode response at low frequencies, and the grain boundary response at mid-frequencies. Grain interiors show as semicircular impedance arcs when plotted on the complex plane, and sample-electrode responses of hot single crystals and of hot dry rocks are exhibited as depressed arcs. In comparison, monofrequency measurements contain no information to identify the source of the response; at 1 kHz they detect only the resistance sum of grain interiors and grain boundaries and at low frequency (≤ 1 Hz) are likely to sense all three components. The major experimental problem is to find electrodes that make good contact with the sample and that are stable with time. The effect of pressure (10 kbar, 300–800 °C) is to diminish the resistance associated with grain boundaries and the sample-electrode interface, in the laboratory and presumably in nature. Monofrequency measurements at 1 bar may underestimate the conductivity of rocks at similar temperature but higher pressure.

A network of electrical elements is presented for use in interpreting impedance spectra and conductive paths in hot or cold, wet or dry, minerals and rocks at any pressure. In dry rocks, a series network path predominates; in wet rocks, aqueous pore fluid and crystals both conduct. Finite resistance across the sample-electrode interface is evidence that electronic charge carriers are present at the surface, and presumably within, the silicate minerals and rocks measured.

Introduction

The basic objective of the research reported in this paper is to understand what is sampled by an impedance spectrum and consider how this new knowledge affects the use of electrical conductivities, measured in the laboratory, to interpret low-frequency electromagnetic responses of the deep crust. The approach is to explore the nature of representative impedance spectra of hot, dry pyroxenes and olivine, measured under a range of physical conditions, and to relate characteristic features to pathways for, or barriers to, conduction. In the future we will systematically summarize our measurements in terms of electrical networks and show how the resulting resistances and dielectric properties vary with changes in the thermodynamic conditions that prevail in the deep crust.

Traditional electrical conductivity measurements of hot minerals and hot dry rocks have been made at a single frequency, assuming that conductivity is independent of frequency at all temperatures and pressures. For instance, Duba (1972, at 1.0 kHz and 30 V), Duba et al. (1974, at 1.0 kHz), Huebner et al. (1979, at 1.0 kHz), Hinze et al. (1981, at 1.6 kHz), Lastovickova (1987, at 60 V, presumably DC), and Shankland and Duba (1990, at 1.0 kHz) measured minerals in this way, and Lee et al. (1983, at 1.592 kHz), Cermak and Lastovickova (1987, using 60 V DC), and Constable and Duba (1990, at 1 kHz) measured rocks.

Data supporting the frequency independence of the conductivity of hot, dry samples are rarely presented. Duba (1972) assumed that olivine conductivity would be independent of frequency. Huebner et al. (1979) stated that conductivity was independent of frequency over the range 0.05–10 kHz but did not justify the assertion. Lee et al. (1983) made exploratory measurements over the frequency 0.2–50 kHz; although they reported that the frequency dependence of the conductivity increased with increasing conductivity, they did not indicate the magnitude of the dispersion. Schock et al. (1989) measured olivine conductivity at 0.1, 1.0, and 10.0 kHz and stated that they did not observe any dependence of conductivity on frequency. Wanamaker and Duba (1993) similarly measured the resistance of olivine at 0.1, 1.0, and 10.0

kHz, found a "small apparent frequency dispersion at low temperatures (high impedance) . . . at 10^4 Hz," but only presented 1.0-kHz data. Lastovickova (1991) showed that the measured conductivity of tourmaline is significantly greater at 1 kHz than at DC and that this effect decreases with temperature. Huebner and Voigt (1988) showed representative plots of impedance vs. frequency for diopside; at 1225 °C the impedance of iron diopside increases markedly below about 10 Hz. These reported changes of conductivity with frequency suggest the use of caution when extrapolating high-frequency laboratory data to the low frequencies used in field geophysics. Our results show that, in general, conductivity depends markedly on frequency.

Impedance spectroscopy (IS) is widely used by materials scientists to study the electrical and microstructural properties of ceramic and metal-organic electrolytes (see the comprehensive review by Macdonald, 1987). The properties of these electrolytes differ from those of rock-forming silicates in several respects. Electrolytes are good ionic conductors, whereas most silicate minerals are poor conductors of either ions or electronic charge. Few impedance spectra of electrolytes have been measured at >800 °C, whereas most crustal silicates are so poorly conducting that few measurements of single crystals have been made at <800 °C. Glassy binders and grain-boundary phases generally impede ionic conduction between grains of electrolytes, whereas grain boundaries in aggregates of minerals may enhance electronic and ionic conduction. We will show that, despite these differences, IS can yield significant information about crustal materials.

BASIC CONCEPTS OF IMPEDANCE SPECTROSCOPY

Fundamentals

Electrical responses of solids and sample-electrode systems are complex functions requiring, for complete description, a real and imaginary component at each frequency. In the case of impedance (Z), the real and imaginary components Z_r and Z_i are the resistance (R) and reactance (X), respectively. The impedance spectroscopy technique measures the frequency dependence of each component.

Impedance is the opposition to flow when an AC electrical signal is passed through the material of interest. Each measurement is collected at a single frequency and contains two kinds of information, electromotive force (E, in volts) and current (I, in amperes), but E and I are generally not in phase (Fig. 1). The elapsed time by which the voltage maximum differs from the current maximum is measured in units of angular frequency (ω in degrees or radians). Negative values of the phase (θ) indicate that the current wave form leads that of the voltage; this case is common and is caused by a capacitance or dielectric response in the sample, sample cell, or measuring circuit. An impedance spectrum consists of a set of measurements at many frequencies. The spectrum can be visualized in the complex (orthogonal) representation (Fig. 2a), in which the real (Z_r) and imaginary (Z_i) terms of

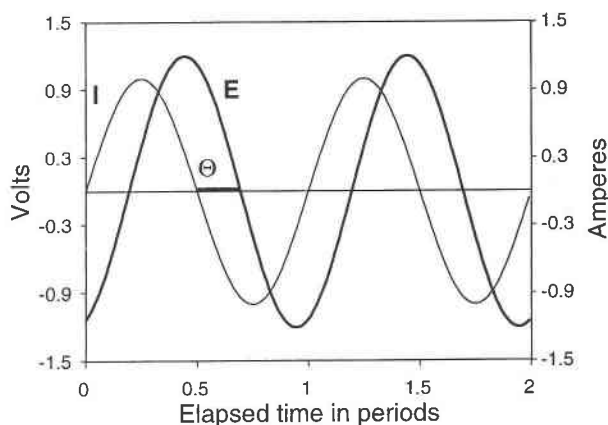Fig. 1. Current (I) and voltage (E) plotted against elapsed time in periods (one period = $1/f$ Hz) for a circuit containing resistance and capacitance. The current leads the voltage by the phase θ. One period is 360° or 2π radians.

the impedance are plotted against log frequency, or in the equivalent polar representation (Fig. 2b), in which log magnitude of the impedance ($\log|Z|$) and the phase are plotted against log frequency (log of f in Hz). The representations are related by the equations

$$\tan \theta = \frac{Z_i}{Z_r} \qquad (1)$$

and

$$|Z|^2 = Z_r^2 + Z_i^2. \qquad (2)$$

Obviously, it is important to state the nature of the reported value, $|Z|$ or Z_r, because, in general, $|Z| \neq Z_r$. In measurements of hot, dry materials, only Huebner and Voigt (1988) were specific, stating that they reported $|Z|$, the magnitude of the impedance, at whatever frequency θ was a maximum ($\theta \approx 0$), thereby minimizing the Z_i component ($|Z| \approx Z_r$).

Impedance can be converted to admittance, complex dielectric constant, or the complex electric modulus function (see Hodge et al., 1976; Hurt and Macdonald, 1986) for numerical modeling and plotting. We used the impedance representation because we measured impedance and found that the other or transformed representations did not as clearly reveal in complex-plane or magnitude-frequency plots the multiple relaxations or processes of conduction that we found in our samples. Three impedance projections were particularly useful in our work: the complex plane plot of $-Z_i$ and Z_r (Fig. 2c); the Bode-magnitude plot of $|Z|$ vs. log f (Fig. 2d), and the Bode-phase plot of log f vs. θ (Fig. 2f). Note that frequency increases toward the left in the complex plane, whereas frequency increases to the right in the other two diagrams.

Basic components

The description of impedance spectra is simplified if we think of them as representing responses of networks that can be decomposed into simple components or pairs
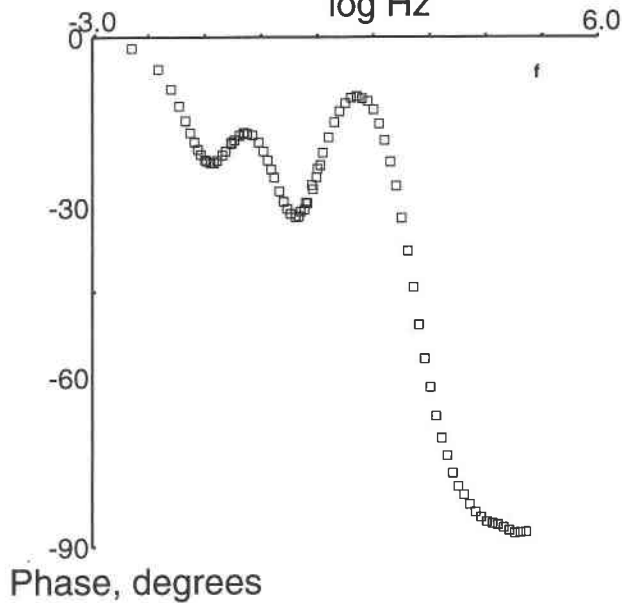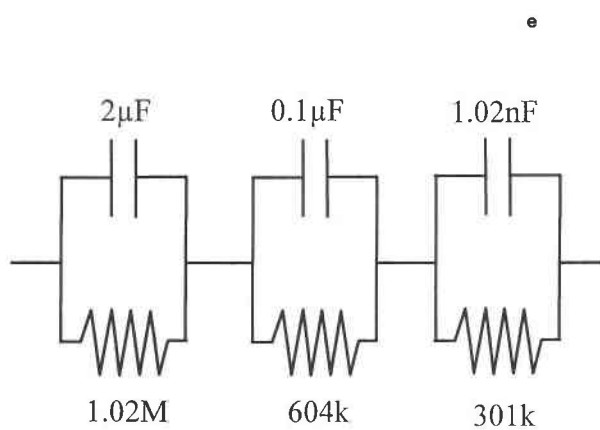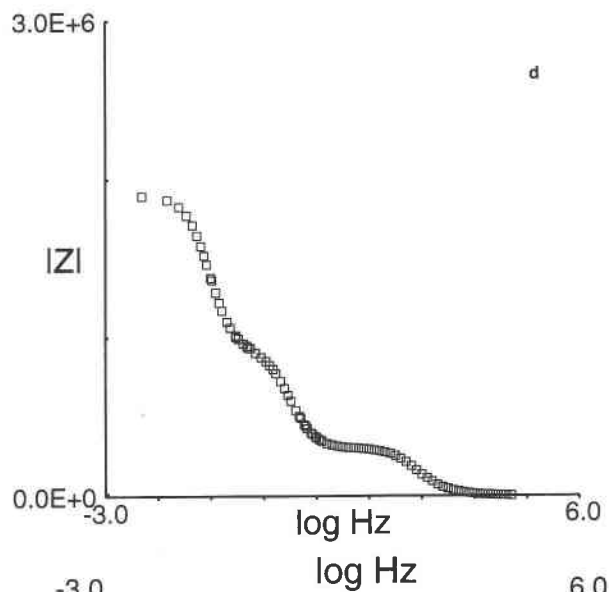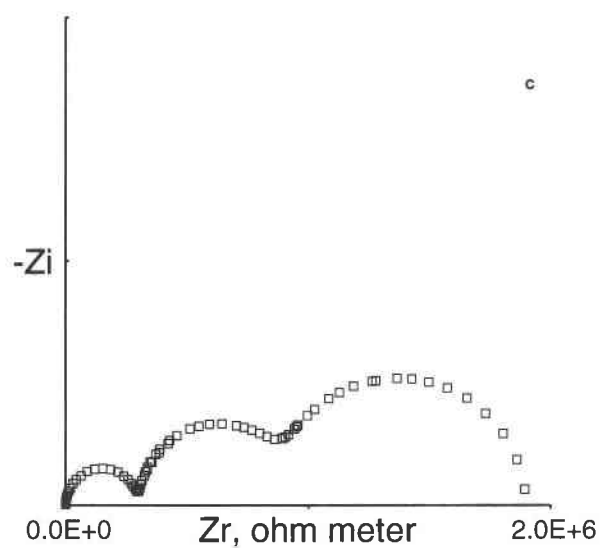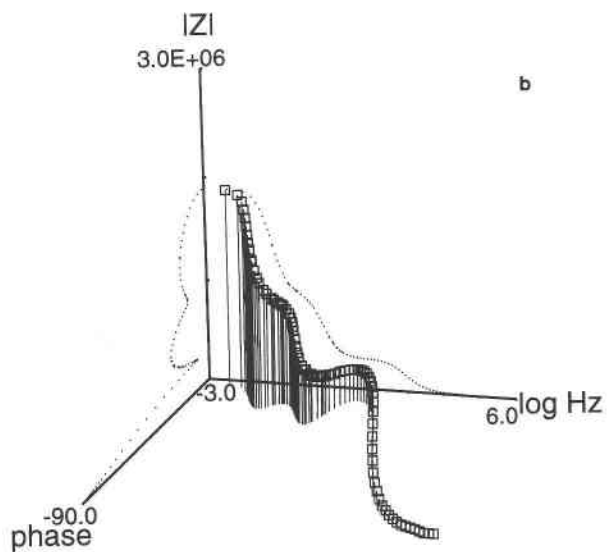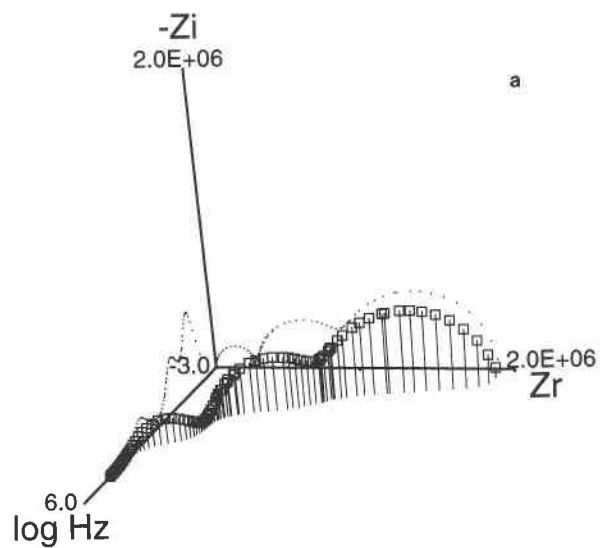
of components, each with a characteristic response. The simplest component is a resistor that obeys Ohm's law, $R = E/I$. The response is independent of frequency; in the complex plane, the response is a point on the real axis (Fig. 3a). The response of an ideal capacitor (a capacitor having a single time constant or relaxation frequency) appears as a vertical line in the complex plane; with decreasing frequency, values of Z_i become more negative. If a capacitor is connected in series with a resistor R, the vertical line intersects Z_r at R (Fig. 3c). The response of a simple circuit, consisting of an ideal resistor and an ideal capacitor connected in parallel, and which we will designate a parallel RC circuit, is an arc centered on the real axis (Fig. 3e) with Z given by

$$Z = \frac{R}{1 + RCi\omega}. \qquad (3)$$

Charge flows through the resistor at all frequencies. Charge accumulates on, but does not actually flow across, the plates of the capacitor; the rate of charging decreases with time. At high frequencies charge flows into the plates of the capacitor which appears to conduct; at low frequency little charge flows into the plates, and the capacitor appears more insulating. At high frequency the impedance is determined by the capacitor, and at low frequency the impedance is that of the resistor. The arc extends from the origin (high frequency) to a point on the real axis corresponding to the value of R (low frequency). When the Z_r and Z_i axes are scaled to the same intervals, the arc is a true semicircle. If the RC is combined with a series resistor R and a series capacitor, the arc is displaced R to the right, along the real axis, and terminates in a vertical line (Fig. 3b). Thus, the spectral response reflects the combination of contributing components.

If three RCs are connected in series (Fig. 2e) and the frequency is swept through a wide range, the resulting spectrum can be shown in the two equivalent representations (Fig. 2a and 2b). Each RC projects onto the complex plane as an arc centered on the real axis (Fig. 2c); the width of each arc is related to the corresponding resistance term R in an equation similar to Equation 3. In this example of a real spectrum in which the semicircles overlap, we made the three relaxations distinct by choosing component values that give widely separated time constants. The highest points on the semicircles (minimum Z_i) in the complex plane correspond to the steepest points of the spectrum in the Bode-magnitude projection (Fig. 2d) and to phase minima in the Bode-phase plot (Fig. 2f). These points correspond to angular frequencies,

$\omega = 1/RC$. Thus if R is fixed, increasing the capacitance C moves the steep slope in the Bode-magnitude plot (Fig. 2d) to lower frequencies (to the left). In the complex plane (Fig. 2c) the points slide leftward along the arcs toward the origin. The interplay of R, C, f, and Z can also be seen if R is decreased (as might be the result of increasing the temperature). The points slide toward lower frequency in the complex plane. For a given frequency range, a high-frequency arc that is completely resolved at low temperature may appear incomplete at high temperature. Similarly, a measurement frequency that falls on an impedance plateau (Fig. 2d) and thus appears independent of frequency (over a limited frequency range) might no longer be on the plateau at higher or lower temperatures, thereby becoming frequency dependent. Raistrick et al. (1976, p. 1474–1475) showed that monofrequency measurements, combined with the assumption of frequency independence, can lead to incorrect values of conductivities and activation energies. (For an illustration of this point involving the complex plane, see Knight et al., 1985, their Fig. 9.)

Points at or near the Z_r axis (Fig. 2c) correspond to plateaus in Figure 2d and maxima in Figure 2f; they are points at which $Z_i \sim 0$. Impedances measured at these points have been called DC resistances, even though the measurement frequencies may be finite (and even quite large). It is ambiguous to speak of a DC resistance unless the form of the low-frequency response has been investigated with measurements at a variety of frequencies.

CPE and ZARC

Real components deviate from ideal behavior in having a distribution of time constants, and impedance arcs of natural materials can deviate from a semicircular shape. Several authors have tried to relate the shape of an impedance arc to mathematical models having a distribution of relaxation times and to physical theory; Macdonald and Potter (1987) review some of the possibilities. We will approximate nonideal behavior by replacing the equation describing an ideal capacitor with the equation:

$$Z = \frac{1}{C(i\omega)^\phi}. \qquad (4)$$

If the capacitor is ideal, $\phi = 1$. If there is a distribution of relaxation times, ϕ is <1. (Experimentally, we find that $\phi = 0.98$–1.00 for networks of resistors and capacitors but that ϕ can be as low as 0.15 for natural materials.) Although the distributed response is not strictly that of a capacitor, we will, for convenience, call C a capacitance,

---

←

Fig. 2. Different plots of a single measured impedance spectrum. (**a**) Real, imaginary, and frequency space (f increases toward the reader), with projections onto the bounding planes. (**c**) Complex plane, real vs. imaginary parts of the impedance. Here and in all complex-plane plots presented in this paper, the $-Z_i$ axis has the same scale as the Z_r axis. The frequencies at which individual data were measured increase from right to left. (**b**)

Magnitude, phase, and frequency (phase θ increases toward the reader), showing projections onto the bounding planes. (**d**) Projection of **b** backward parallel to θ showing magnitude vs. frequency (sometimes called a Bode-magnitude plot). (**f**) Projection of **b** downward parallel to the magnitude, showing phase θ and frequency (sometimes called a Bode-phase plot). (**e**) Network used to acquire these spectra.
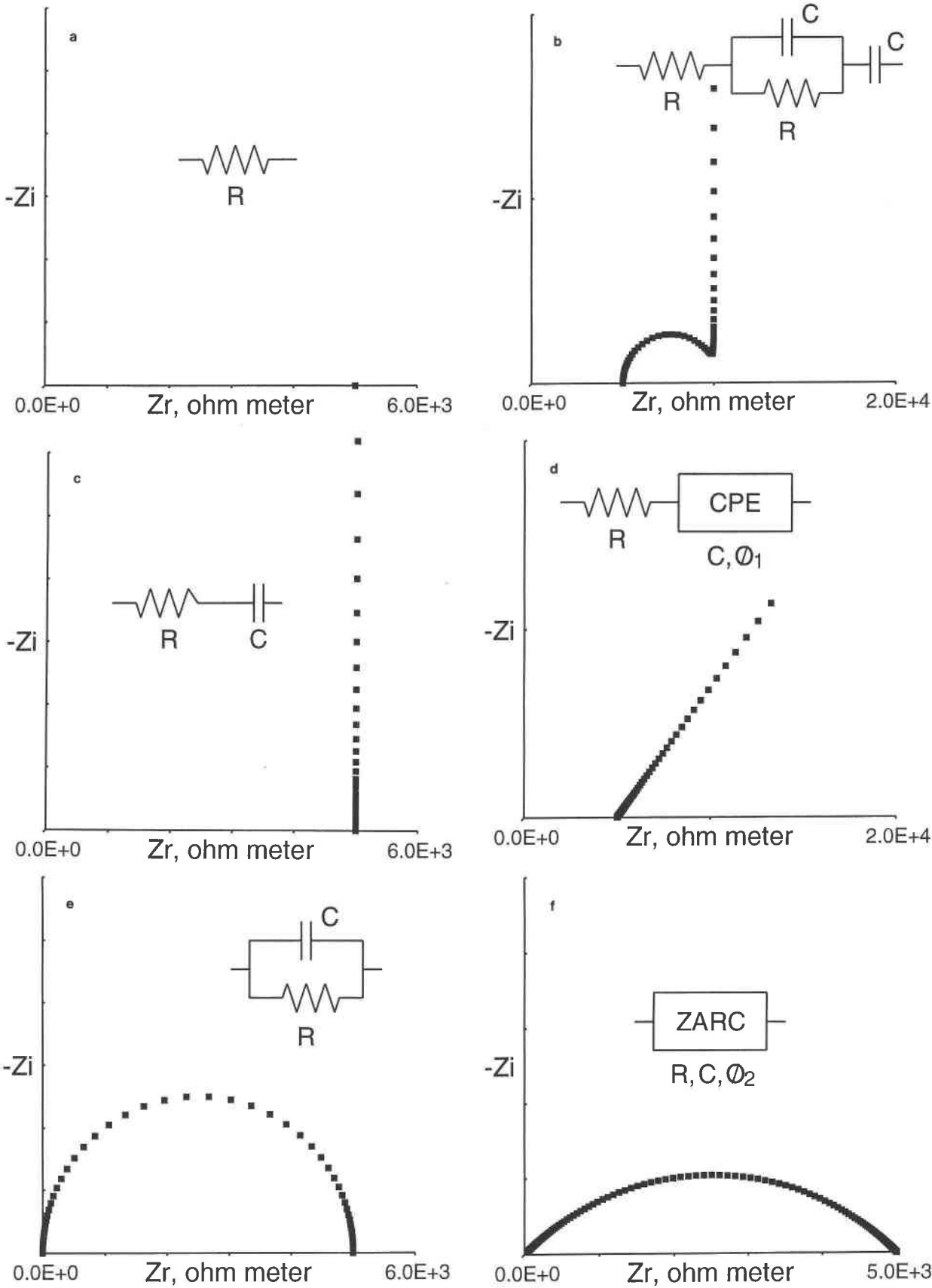
with units of Farads. The corresponding impedance becomes an inclined line (Fig. 3d); $-Z_i$ and Z_r both increase with decreasing frequency and $Z_i/Z_r = \tan \theta$ is constant (thus the term constant-phase element or CPE). The corresponding parallel combination of an ideal resistor and CPE element is called a ZARC; its impedance is given by

$$Z = \frac{R}{1 + RC(i\omega)^\phi}. \tag{5}$$

When $\phi < 1$, the center of the impedance arc lies below the Z_r axis, and the arc appears depressed (Fig. 3f). The slopes in the Bode-magnitude plot become less steep, and the valleys in the Bode-phase plot broaden. The ZARC response approaches that of a CPE as $R \to \infty$.

Models

The literature of materials characterization abounds with suggestions about what might be revealed by impedance spectra. For instance, Macdonald (1976) envisioned a general model with bulk conduction, grain boundary resistance, chemical reactions, surface absorption and reaction, and diffusion. Ideally, five relaxations could be distinguished if their time constants were distinct. Research on high-temperature (and thus dry) polycrystalline electrolytes that incorporate a binder provides a better analogy for hot dry rocks. Chu and Seitz (1978), Kleitz et al. (1981), Gerhardt and Nowick (1986), and Matsui (1986) all hypothesized impedance spectra with three arcs due to grain interiors (at highest frequency), grain boundaries, and electrodes (lowest frequency). However, the response of electrodes that are totally blocking with respect to the charge-carrying species should be a CPE. Nonideal behavior due to a distribution of relaxation times may provide additional clues to the identity of the arcs. Sample heterogeneities and interfaces that deviate from infinitely thin planes perpendicular to the direction of current flow are a possible cause. Thus, grain boundaries in a sample could lead to a depressed arc, and the response of a sample-electrode interface that suffers from heterogeneously distributed metal, air gaps, and polishing relief would be nonideal. In contrast, the response of the interiors of homogenous grains should give a response that is close to ideal ($\phi \sim 1$).

PREVIOUS IS OF EARTH MATERIALS

There are few previous IS measurements of Earth materials. Olhoeft (1985) showed Bode and complex-plane plots of graphite and niccolite. Lockner and Byerlee (1985) measured the room-temperature impedance of sandstone saturated with a dilute aqueous solution of KCl over the

frequency range 1 mHz–1 MHz. The measurements reflect the presence of conductive liquid along the grain boundaries and its interaction with the electrodes. Increasing the confining pressure increased the impedance; this behavior was attributed to closing the grain boundaries, decreasing the cross-sectional area of solution. Sato and Ida (1984) determined the impedance of gabbro over the range 32 mHz–10 kHz. Below 1100 °C, Z_r decreased and Z_i increased with frequency, a pattern that might be explained as the right or low-frequency side of an impedance arc (see Fig. 3e and 3f). Above 1100 °C, Z_r and Z_i both decreased with increasing frequency, a pattern that might represent the left or high-frequency side of an arc. These authors concluded that interconnected melt controlled the high-temperature response. Abelard and Baumard (1980) measured the impedance of synthetic forsterite with excess silica, at 527–706 °C. They observed one perfectly semicircular feature in the impedance plane and attributed it to the bulk sample. A second semicircle appeared under some conditions, but Abelard and Baumard did not decide whether it was caused by a sample microstructure (such as grain boundaries) or electrode interactions. Roberts and Tyburczy (1991, 1993), using a strategy remarkably similar to ours, used two- and four-electrode techniques to identify grain-interior, grain-boundary, and sample-electrode relaxations in polycrystalline olivine, 800–1400 °C. However, because their samples were 0.5–1.0 mm thick, we cannot be sure that their four-electrode configuration was comparable with ours. Knight (1983) used the IS technique to study the behavior of water and water vapor in partially saturated porous sandstones at room temperature. She observed almost semicircular arcs. Huebner and Voigt (1988) plotted impedance spectra of two clinopyroxenes at high temperatures in the Bode-magnitude and Bode-phase representations; most measured plates of diopside ($Di_{97.3}Hd_{2.7}$) showed one relaxation (and one plateau) above about 500 Hz, but diopside ($Di_{87.3}Hd_{12.7}$) showed a relaxation between two plateaus. They plotted $\log|Z|$, unfortunately obscuring detail that might have been revealed had they plotted $|Z|$. It is features such as these that we attempt to characterize in this report.

METHODOLOGY AND SAMPLE DESCRIPTIONS

We had available three instrumental configurations.

(1) The first configuration was the apparatus available to Huebner and Voigt (1988), which consisted of an electrometer, potentiostat, lock-in amplifier, and microcomputer. The internal oscillator of the lock-in amplifier was used to drive the power amplifier (in the potentiostat)

←

Fig. 3. Calculated complex-plane plots illustrating the impedance responses discussed in text. Component values: $R = 5000\ \Omega$, $C = 1\ \mu F$, $\phi_1 = 0.62$, $\phi_2 = 0.50$. (a) Resistor. (c) Resistor in series with ideal capacitor; angular frequency ω increases downward. (e) RC: parallel resistor and ideal capacitor; ω increases to left. (b) RC in series with resistor (R) and ideal capacitor; ω increases downward. (d) CPE (constant-phase element) in series with resistor (R); ω increases toward origin. (f) ZARC (impedance arc or resistor in parallel with a CPE); ω increases to left.

TABLE 1. Sequence and duration of measurement ranges using potentiostat, lock-in, and FFT techniques

Stage	Name	Frequency interval	Points	Cycles	t
Four-stage sequence, 104 impedance measurements					
1	LOCK-IN	5.010 Hz–100.0 kHz	44	1	14 min
		current ranging			2.8 h
2	FFT E-4	0.1000–11.3 mHz	20	4	11.3 h
		FFT calculations			2 min
		current ranging			50 s
3	FFT 0.1	0.1001–11.31 Hz	20	5	50 s
		FFT calculations			2 min
		current ranging			10.2 min
4	FFT 0.005	0.005 001–0.5651 Hz	20	5	16.2 min
		FFT calculations			2 min
Five-stage sequence, 124 impedance measurements					
1	LOCK-IN	5.010 Hz–100.0 kHz	44	1	14 min
		current ranging			5.55 h
2	FFT 5 E-5	0.05000–5.650 mHz	20	3	16.7 h
		FFT calculations			2 min
		current ranging			10.2 min
3	FFT 0.005	0.005 001–0.5651 Hz	20	5	16.2 min
		FFT calculations			2 min
		current ranging			50 s
4	FFT 0.1	0.1001–11.31 Hz	20	5	50 s
		FFT calculations			2 min
		current ranging			8.5 h
5	FFT E-4	0.1000–11.30 mHz	20	4	11.3 h
		FFT calculations			2 min

Fig. 4. Electrodes and instrumentation. Samples are placed between Ir plate electrodes having leads $E1$ and $E4$. SEI is sample-electrode interface. Source applies an alternating current to the outer electrodes. Ammeter A measures the current passing through the sample; voltmeter V2 measures the voltage across the sample cell (including Ir electrodes). Long samples have inner Pt electrodes connected by leads $E2$ and $E3$ to voltmeter V1 for true four-electrode measurements. A, V1, and V2 share a common time base, making possible measurements of complex voltage and current.

with a simple sine waveform over the range 5 Hz–100 kHz; the output of the amplifier was delivered to the two current electrodes attached to the sample. The potentiostat returned two (multiplexed) signals to the lock-in; the voltage across the sample and the voltage across a current-ranging resistor contained within the potentiostat. The lock-in compared these two signals with its internal reference signal and reported voltage, current, and phase. For low-frequency spectra (50 μHz–11 Hz), the microcomputer calculated a multisine voltage waveform, which was applied to the sample as an analogue waveform by the potentiostat. The potentiostat digitally measured (as a function of time) the current passing through the sample but never measured a voltage waveform. The measured current waveform was used in an FFT algorithm to extract the real and imaginary terms of the current. Finally, these were combined with the calculated applied-voltage waveform to obtain the impedance at each frequency. The voltage generated by the potentiostat was increased from that generated by Huebner and Voigt's (1988) procedure such that the maximum peak to peak voltages encountered were about 370 mV at 4 kHz using the lock-in technique and about 4 V using the FFT technique. Use of these higher voltages markedly improved the agreement over the frequency range (5–11 Hz) in which the high-frequency lock-in and low-frequency FFT techniques overlapped and improved the quality of the spectra by decreasing the noise. Spectra consisted of either 104 or 124 points, depending on whether four or five segments of data acquisition were used (see Table 1).

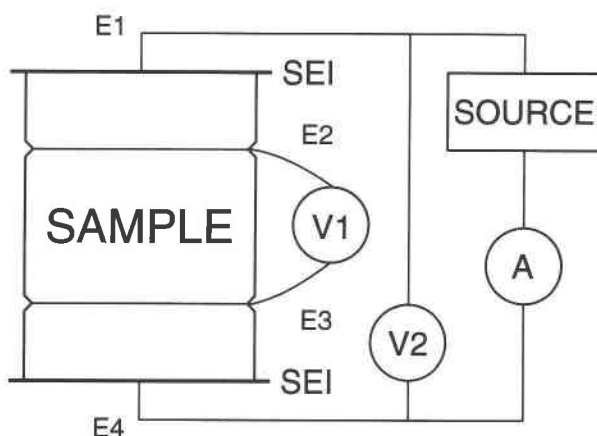(2) We modified the potentiostat in three respects to make possible true four-electrode measurements in which electrodes used to measure voltage are distinct from electrodes used to stimulate the sample (Fig. 4; also see Olhoeft, 1979, and Lockner and Byerlee, 1985). (a) We moved the output of the electrometer from the power amplifier feedback circuit to an analogue to digital converter (ADC), making possible actual voltage measurements of the low-frequency multisine waveforms. We maintained the existing path from the electrometer to the voltage-current multiplexer leading to the lock-in analyzer (for high-frequency measurements). (b) We connected a new operational amplifier to the counter and working electrodes to provide necessary feedback to the power amplifier, thereby making possible the use of the electrometer to measure any voltage that we chose. (c) We modified the software so that the potentiostat actually measures the voltage wave form and so that measured current and measured voltage are used as input for the FFT calculation.

(3) We acquired an impedance analyzer (Schlumberger Model 1260)[1] for use over the frequency range 10 μHz–32 MHz; a single sine is used even at the lowest frequencies. This instrument applies a controlled voltage stimulus to the sample and digitally measures three responses, the current passing through the sample and two voltages. We did not find any systematic relationship between stimulus amplitude and measured impedance, as expected for silicates that are good insulators with high breakdown voltages (dielectric strengths). We used the maxi-

---

[1] Use of trade names and names of suppliers of materials and equipment is for descriptive purposes only and does not imply endorsement by the U.S. Geological Survey.

mum possible amplitude (6 V peak to peak) to improve the signal to noise ratio. Impedance is extracted using correlation frequency response analysis (Wellstead, 1983a, 1983b). For each frequency it is possible to obtain simultaneously two- and four-electrode measurements, both reported as Z_r and Z_i. Most spectra consisted of about 173 data points over the frequency range 400 μHz–10 MHz.

For all measurements made at 1 bar, the sample cell ceramics and Ir outer electrodes were as described in Huebner and Voigt (1988), but the electrical leads were modified to permit four-electrode measurements. Four individually shielded coaxial leads, each 1.0 m in length, led to the furnace hot spot. The inner and outer conductors were Pt wire and tube (within the muffle tube) brazed to Cu wire and braid (outside the base of the muffle tube). Two leads, designated counter and working, connected the Ir (outer) electrodes with the waveform generator and current measurement circuits and, as needed, the electrometer or a voltage analyzer. When making true four-electrode measurements, the other two leads connected inner Pt electrodes (which girdled cylindrical samples, Fig. 4) to the electrometer or the second voltage analyzer.

The sample-electrode cell assembly was positioned on (and supported by) a vertical high-purity alumina rod. A similar upper rod, weighing about 100 g, was free to rest on the upper Ir plate, gently forcing the metallic electrodes and the sample together. We intended that the electrodes would be blocking to all mobile species except electrons; in reality, the electrode-sample interface probably did not exclude vapor, thereby probably permitting the passage of O into (and out of) the upper and lower surfaces of the mineral plates.

Mixtures of CO and CO_2 gases specified the f_{O_2}, using techniques described by Huebner (1987). The range of temperature and f_{O_2} variation during collection of a spectrum was <1 K and (except at gas mixing ratios <0.1 vol% CO) no more than 0.02 log f_{O_2} unit. The thermocouple circuit was calibrated against the melting point of Au, 1341 K; the correction was 9 K at the beginning and 6 K at the midpoint and end of the study. The sample, electrodes, and zirconia cell (O_2 sensor) with thermocouple were positioned within the furnace hot spot (± 1 K) at all temperatures. The cell was assumed to obey the Nernst equation (electronic conductivity absent) and the cell emf was recorded to 0.1 mV. The cell reference gas was air, supplied by an aquarium pump equipped with an overflow bubbler containing butyl pthalate; the reference f_{O_2} was assumed to be a constant 0.209 bar, although it surely fluctuated with ambient atmospheric pressure. The corresponding accuracies were estimated as ± 5 K and ± 0.1 log f_{O_2} unit.

Impedance spectra at 10–20 kbar were obtained in a 1-in. piston-cyliner apparatus, using a NaCl assembly (Fig. 5). Cylinders of clinopyroxenite, 2.22–8.01 mm long, were machined to a diameter of 8.03 mm and placed within a vertical silica-glass sleeve having an 8.10-mm i.d., an 11.51-mm o.d., and a 30.48-mm length. Pt disks 0.025
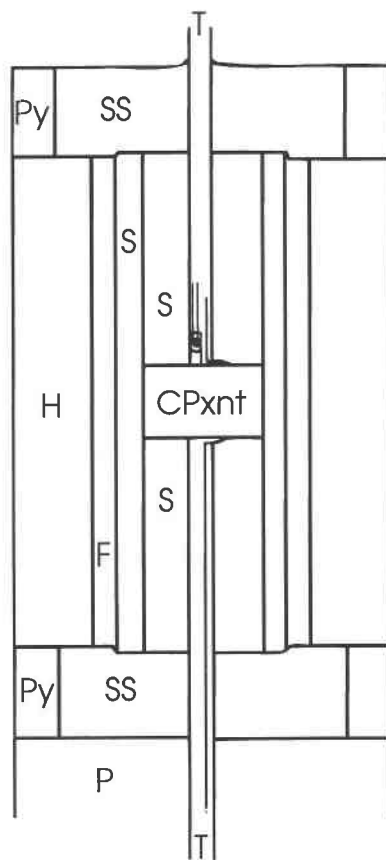

Fig. 5. Piston-cylinder assembly used for high-pressure measurements of clinopyroxenite. The sample (CPxnt) is insulated from the graphite furnace (F) and stainless-steel plugs (SS) with a silica-glass sleeve and plugs (S). Alumina tubing (T) insulates the thermocouple and electrode leads (top) and the lower electrode lead (bottom). H is NaCl sleeve; Py is pyrophyllite; P is W carbide piston (not part of the consumable assembly). Not shown: Pb foil surrounding H, Pt foil electrodes at upper and lower surfaces of sample. Diameter = 0.02540 m, length = 0.04625 m.

mm thick placed at the ends of the sample served as electrodes. Silica glass plugs having an 8.09-mm o.d. and a 1.60-mm i.d. were placed above and below the Pt electrodes so that the length of the inner stack exceeded the length of the sleeve by 0.2–0.3 mm. This assembly was placed in a graphite sleeve heating element having an 11.5-mm i.d. The central portion of each of the stainless steel base plugs, 11.5+ mm in diameter, was milled to a depth of 0.51 mm to receive the silica sleeve. The lower Pt lead led from the lower Pt electrode, downward through the silica plug, baseplug, and piston; insulation was provided by an alumina tube and Teflon tubing. Similarly, the upper electrode lead and two thermocouple leads led upward through the upper silica plug, steel base plug, and the steel cylinder (called a hockey puck). No glue or cement was used to immobilize the experiment parts during assembly because we found that the resulting volatiles

TABLE 2. New chemical analyses, pyroxene and olivine

	K*	MF1**	Mal†	DK7‡	DK8§	SC§
			wt%			
SiO_2	47.59	55.24				
P_2O_5	0.01	n.d.				
TiO_2	2.00	0.04				
Al_2O_3	9.75	1.87				
Cr_2O_3	0.01	0.47				
MgO	13.20	31.27				
FeO	8.48	10.62				
NiO	n.d.	0.28				
MnO	0.19	0.18				
Na_2O	1.42	0.03				
CaO	18.04	0.20				
ZnO	n.d.	n.d.				
Total	100.68	100.22				
			ppm			
Sc	61			1.1	1.0	2.7
Cr	23		1980	5.2	4.4	192
Co	34		20	0.2	0.2	112
Ni	<100		350	<4	<3	2580
Zn	22		44	17	15	46
Sr	<400		100	30	29	<300
Ba	39		<40	<15	<11	<12
La	3.0		0.2	0.4	0.8	0.025
Ce	8		<9	1.7	3.0	<2
Nd	8		<3	2.1	1.8	<1
Sm	4.0		0.2	0.52	0.58	<0.003
Eu	1.4		0.07	0.11	0.12	<0.02
Tb	0.9		0.07	0.09	0.09	<0.04
Yb	1.8		0.3	0.39	0.37	<0.03
Lu	0.2		0.07	0.07	0.06	<0.005
Zr	<400		<140	31	<6	<90
Hf	2.7		0.14	0.55	0.41	<0.1
Th	<0.8		<0.8	0.07	0.07	<0.2
U	<0.2		0.1	<0.09	<0.07	<0.05

Note: n.d. = not determined.
* Forty microprobe points on six plates; one INAA analysis.
** Eight additional microprobe analyses on one plate (see Huebner et al., 1979).
† Average of four new INAA analyses (see Huebner and Voigt, 1988).
‡ One new INAA analysis (see Huebner and Voigt, 1988).
§ One INAA analysis.

decomposed to films of C near the hot spot, causing low-resistance paths between the upper electrode and the thermocouple circuit. Spectra were acquired with the impedance analyzer. AC coupling protected the analyzer (in case graphite from the furnace made contact with the electrode leads) but limited the effective lower frequency to about 20 mHz. Results reported below met the following criteria. (1) Impedance spectra varied systematically and reversibly with temperature; we also found that we could successfully increase or decrease pressure during an experiment. (2) The resistance, measured between the electrode leads with a DVM, was low compared with the resistance between either electrode lead and any of the power and thermocouple leads. (3) We did not find the impedance spectra to be perturbed at 60 Hz or at the harmonics, even though the power to the furnace was phase-angle-fired 60 Hz AC (Huebner, 1987, p. 35). (4) The thermocouple circuit was similarly isolated from the power leads. (5) The graphite sleeve did not expand, bulge, or fracture during the experiment.

To compare spectra, we chose three clinopyroxene and one orthopyroxene single crystals, two olivine single crystals, sintered aggregate prepared from diopside, and a clinopyroxenite.

The DK7 diopside crystal is from DeKalb, New York; other crystals from the same lot were subsequently assigned U.S. National Museum of Natural History acquisition numbers R18682–R18684. Chemical and X-ray data were given by Huebner and Voigt (1988, their Tables 1 and 2). New trace element analyses (Table 2) of crystal DK8 augment the earlier data. (DK8 is from the same lot as DK7 and could not be distinguished from DK7 by microprobe analysis or cell dimensions.) For this study we measured DK7a2, a (100) plate that had not previously been measured, and four disks of diopside aggregate prepared by sintering <100-mesh dry powder of DK7 diopside in a graphite crucible at 950 °C and 10 kbar for several hours. Sintered cylindrical plugs (DK7sp, DK7sp2) fractured perpendicular to the cylinder axis on the *P-T* quench, forming convenient disks of surprisingly uniform thickness, requiring only gentle grinding to make plane-parallel surfaces.

MAL, the hedenbergitic diopside, is a previously unheated (100) plate of the same crystal that was described and measured by Huebner and Voigt (1988). The compositions of DK7 and MAL are related principally by the substitution $Mg \rightleftharpoons Fe^{2+}$. New trace-element data by instrumental neutron activation analysis (INAA; see Baedecker and McKown, 1987) augment the chemistry presented by Huebner and Voigt (1988).

Kangan clinopyroxene (augite from Kangan, India) is related to diopside by the substitution of Fe^{2+}, Al, and Ti for Ca, Mg, and some Si. The augite has cell dimensions $a = 9.701(1)$, $b = 8.851(1)$, $c = 5.2737(9)$ Å, $\beta = 106.55(1)°$, and $V = 434.37(8)$ Å³. Electron microprobe and INAA analyses are summarized in Table 2. G. R. Rossman (personal communication) examined (010) plates of the Kangan augite using infrared spectroscopy; he estimated 0.070 wt% OH^- before heating, of which 97% was lost on exposure to high temperatures in our furnace. Skogby et al. (1990) subsequently reported 0.026 wt% OH for an unheated plate of our material but did not identify the orientation of the plate. We measured plates cut on the perpendicular to the reciprocal axes **a***, **b***, and **c*** and labeled Ka1, etc.

MF1b orthopyroxene was a previously unheated plate cut parallel to the two (010) plates of MF1 that were measured by Huebner et al. (1979). New microprobe analyses are given in Table 2; the microprobe analysis of MF1b revises that of Huebner et al. (1979); in particular, 0.28 wt% NiO was found by the microprobe. Unfortunately, the remaining sample is too small for INAA analysis.

SC2c is a plate of San Carlos olivine, cut on the perpendicular to the **c*** axis, and is immediately adjacent to a plate measured by Wanamaker and Duba (1993). The minor- and trace-element chemistry of the olivines from San Carlos is not well known. We had analyzed by the

TABLE 3. Preparation of samples

Sample	Length (m × 10³)	Effective area (m²)	Area factor (m)	Contact preparation	Location
Ka1	0.8674	1.19814×10^{-4}	0.138128	evPt	se
Kb1	0.59817	5.71043×10^{-5}	0.095465	evPt	se
Kc1	0.84836	5.67019×10^{-5}	0.066837	evPt	se
DK7a(-2)	0.660	5.56014×10^{-5}	0.084245	Ptp	se
DK7sp*	0.4064	7.2954×10^{-5}	0.1795	Ptp	le
DK7sp2	0.4318	2.0195×10^{-5}	0.0468	Ptp	le
MF1b'	0.3226	1.407×10^{-5}	0.04362	Ptp?	se?
SC2c	0.8966	6.105×10^{-5}	0.06809	Ptp	se
CPxnt8	10.09	2.1262×10^{-5}	0.002107	evPt, Ptppf, Irglyc	se, D, D
CPxnt8**	5.08		0.004185		
CPxnt9	10.55	7.6128×10^{-5}	0.007216	evPt, Irglyc	se, D
CPxnt9**	5.077		0.0150		
Synfo85	6.97	2.5292×10^{-5}	0.003629	evPt, Irglyc	se, D
Synfo85**	3.27		0.007735		
Nor1	13.63	8.593×10^{-5}	0.006305	Irec	D
Nor1**	6.23		0.01379		

Note: evPt = evaporated Pt; Ptp = Pt "paint"; Irglyc = slurry of Ir black and glycerine; Irec = slurry of Ir black in dilute solution of ethyl cellulose in toluene; Ptppf = Pt foil with Pt paint making contact with Ir plate electrodes; se = applied to ends of sample; D = applied to inner surfaces of Ir plate electrodes; le = applied to upper surface of lower Ir plate electrode.
* Four pellets.
** Four point.

INAA method a different but, we think, similar crystal of San Carlos olivine. Constituents detected are Fe = 6.2 wt%, Ni = 2580 ppm, Cr = 192 ppm, Co = 113 ppm, Zn = 46 ppm, Sc = 2.7 ppm, and La = 82 ppb.

Synfo$_{85}$ is an imperfect cylinder cut from an elongate, pale yellowish green boule of olivine (Hanson et al., 1991) having an approximate composition Fo$_{85}$Fa$_{15}$ and the label LLL 8V24. The axis of the boule and cylinder is approximately perpendicular to **b** and lies about 10° from **a** in the **a-c** plane. Before cutting, this boule had a fracture parallel to and extending from the central axis to the outer surface. During preparation of our 7-mm-long cylinder, that fracture opened to the opposite side; the two halves were firmly held together with Pt wire that formed the inner electrodes. Because the fracture was parallel to the long axis of the crystal (and the direction of current flow), Synfo$_{85}$ should behave as two single crystals adjacent to each other and having the same orientation.

CPxnt is a pale green, essentially monomineralic granoblastic clinopyroxenite from Sleaford Bay, South Australia. Kirby and Christie (1977) reported no significant preferred orientation, an average grain size of 0.6 mm, and an absence of deformation features. The pyroxene composition is $Na_1Ca_{98}Mg_{79}Fe_{23}Al_2Si_{198}O_{600}$ by our microprobe analysis.

Top and bottom surfaces of the plates and cylinders were ground flat with 600-mesh SiC grit, then polished, finishing with 1-μm alumina on a hard silk lap (to minimize polishing relief, especially with polycrystalline samples), and cleaned ultrasonically in acetone and distilled water. Some samples were cleaned by exposure to Ar plasma in a vacuum evaporator, then coated with a thin layer of evaporated (not sputtered) Pt. A mask shielded the cylindrical surface from Pt vapor. Contact between sample surfaces and the Ir electrode plates was enhanced by painting the ends of the sample or the inner faces of the plates with paint containing suspended Pt. We abandoned the Pt paint when we realized that it was contaminated with Au and that the Pt was preferentially dissolving in the Ir, leaving behind Au-enriched blebs of alloy. Subsequently, we used a slurry of Ir black in glycerine or in a solution of ethyl cellulose and toluene. To prevent the conductive paint from introducing a short circuit by flowing along the sides of the sample, along the grain boundaries of the aggregates, or along the fracture in Synfo$_{85}$, we used a stream of hot air to help dry (and thicken) the paint. In all cases, the organic vehicle evaporated or oxidized so that, following heating, we observed a coating that ranged from a continuous metallic layer to closely spaced, minute blebs of metal.

For the purposes of this investigation, we assumed that all responsive parts of a sample could be scaled volumetrically to a meter cube. All measured impedances were multiplied by a factor A/L (area/length, m²/m) to scale the measurements to units of ohm meters. Factors ranged from 0.1795 to 0.003629 (Table 3). If least-squares fits to raw and scaled spectra are compared, volumetric scaling decreases the resistance and increases the capacitance terms. However, if we wanted to scale a surficial response of a sample (for instance, the contribution of the electrode-sample interaction, which has an unknown but constant thickness), a more appropriate scaling factor would be 1 m²/A, giving a range in factors from 8347 to 71073. Such a scaling increases capacitance terms but does not make a proper correction for the bulk properties.

Parameters describing simple circuits were fitted to impedance spectra using the complex nonlinear least-squares (CNLS) program of Macdonald et al. (1981, 1982). CNLS fitting allows measured spectra to be described in terms of networks of frequency-independent components, such as ideal resistors, capacitors, and inductors, and frequency-dependent (distributed, nonideal) components (Mac-
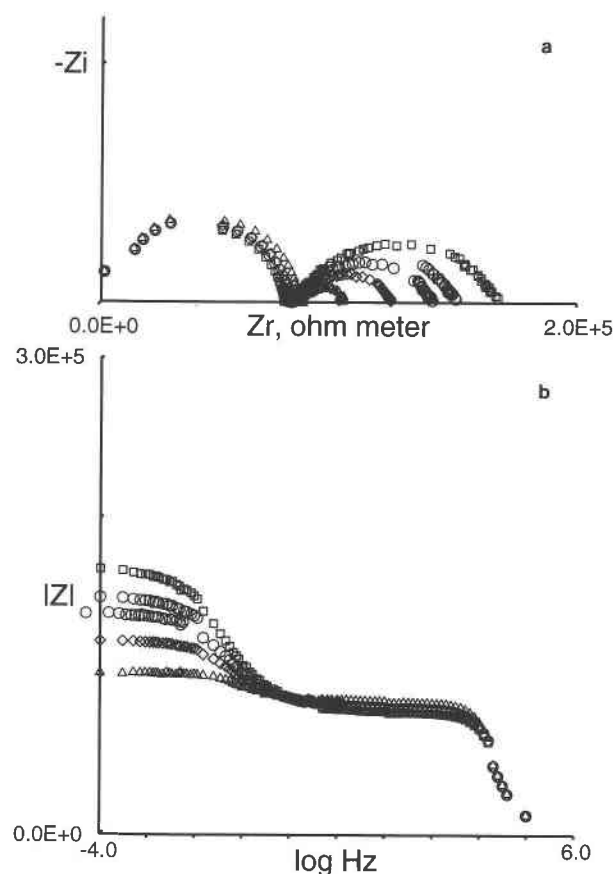
Fig. 6. Time sequence of impedance spectra of a DK7a2 single crystal taken after first heating. Impedance spectra represented by triangles, diamonds, circles, and squares were initiated 5, 33, 53, and 125 h, respectively, after experiment conditions of 1100 °C and log f_{O_2} (in bars) $= -12.0$ were first reached. (a) Complex plane plot. Each spectrum consists of an almost semicircular high-frequency arc (grain-interior response) and a depressed low-frequency arc (sample-electrode interaction). With time, the high-frequency arc decreased slightly in size but the low-frequency arc grew substantially. The double arc at 53 h (circles) appears because the inner data were collected before the outer data. (b) Plot of same spectra in coordinates of impedance magnitude and frequency.

donald and Potter, 1987). CNLS is supplied as a package of Fortran-77 programs; for our work, we combined the program segments into one program and modified the input and output so that we could read data as delivered by the Apple IIe (controller for the lock-in analyzer and potentiostat), fit, and plot the results. The output from the impedance analyzer was converted to the same format. The entire data measurement and reduction process was verified by measuring networks of components, obtaining spectra that agreed in shape with models calculated from the measured networks of components, and in extracting values of resistors and capacitors that agreed with the values of the individual components used to construct the measured networks. The software was further verified by reproducing the complex impedance and

admittance plots of Boukamp (1984), using his refined parameters for his test circuit and for Na_2SnS_3. The emphasis of this paper is on interpreting the spectra by relating shapes or features of the spectra to physical features of the samples. Visual comparison of measured and model (calculated) spectra was greatly assisted by the use of three-dimensional graphics programs (mono and slidmakr), written in Fortran by one of us (J.S.H.) and based upon subroutine calls to Hoops (hierarchical object-oriented picture system, created by Ithaca Software, Inc.).

QUALITATIVE SPECTROSCOPY

To learn the relationships between the shapes of spectra and the physical features of samples, we measured single crystals and clinopyroxenite (polycrystalline) using two- and four-electrode techniques at 1 bar. We hoped to distinguish grain-interior, grain-boundary, and sample-electrode components of the spectra. The clinopyroxenite was measured at high pressure by the two-electrode technique, with the expectation that increased pressure would dramatically change the grain-boundary and sample-electrode responses, helping to confirm the interpretation based on measurements at 1 bar. These relationships between spectral and sample features help us understand what has been measured in the laboratory by geophysicists using conventional electrical conductivity measurement techniques, suggest what is measured by low-frequency soundings in the field, and provide a context for future quantitative analysis of impedance spectra.

The basic model consists of one ZARC for each of the grain-interior, grain-boundary, and sample-electrode responses. We expected spectra of single crystals to have two arcs and those of polycrystalline samples, three arcs.

Clinopyroxene single crystals

Spectra in the complex plane consist of an almost semicircular arc at high frequency and a depressed arclike feature at low frequency. DK7a2 is unique in that the low-frequency feature appears to be a single depressed arc (Fig. 6). Because there are no grain boundaries in the DK7a2 single crystal, we attribute the high-frequency semicircular arc to grain-interior response and the low-frequency arc to sample-electrode interaction. Observed changes in the metallic coatings on the apposed polished sides of the plates, such as the transition from a mirror-like coating to tiny discrete blebs, might be related to the increase with time in the size of the low-frequency arc. Nevertheless, we are surprised that the changes were so symmetrical that the shape of the arc did not change.

The spectrum of Ka1 at 1025 °C and log $f_{O_2} = -12.0$ (Fig. 7) is representative of the other pyroxene single crystals examined by us in that the low-frequency arc is composite. CNLS fitting of this spectrum revealed the following values (arc 1 is at the highest frequency):

	R (ohms)	C (Farads)	ϕ
Arc 1	7721 ± 0.50%	1.1×10^{-9} ± 45%	0.79 ± 5%
Arc 2	8300 ± 7.1%	3.2×10^{-5} ± 5%	0.55 ± 3%
Arc 3	24500 ± 3.0%	2.0×10^{-4} ± 8%	0.64 ± 2%

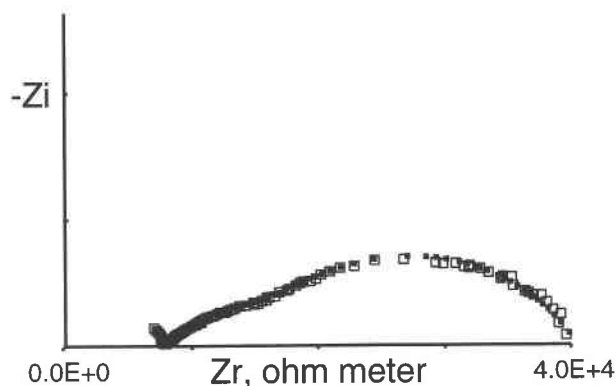Fig. 7. Impedance spectrum of single-crystal Ka1, 1025 °C and log $f_{O_2} = -12.0$. The low-frequency sample-electrode arc is composed of two depressed arcs having different widths (resistances) and unlike time constants. Open squares are measured impedances; filled squares are calculated from the model (see text).

If the entire composite arc is to be attributed to the sample-electrode response, physical differences between the top and bottom interfaces must account for a threefold difference in R and a sixfold difference in C. Because most spectra of clinopyroxene single crystals are best fitted by three ZARCS, one cannot safely conclude that the middle arc of a polycrystalline sample is due to the presence of grain boundaries.

Orthopyroxene single crystal

Before exposure to conditions as reducing as those of the iron + wüstite + vapor assemblage (log $f_{O_2} = -14.0$ at 1050 °C), all spectra of Mf1b could be well described, visually and through CNLS fitting, as a resistor (or arc that lies above the window of available frequencies) and two ZARCs (Fig. 8). We tentatively assign the resistor to the grain-interior response and the two overlapping, depressed arcs to sample-electrode interactions. Following exposure to reducing conditions, two additional relaxations appeared; CNLS fitting improved after an RC and a ZARC were added to the model: R-RC-ZARC-ZARC-ZARC. (Below 950 °C the high-frequency R-RC portion could not be resolved as two elements.) Following measurement, reflected light microscopy revealed trains of highly reflective blebs, <2 μm, that appear to decorate dislocations near the surface. These features were not present before the crystal was heated. We note the 0.33 wt% NiO content of the San Carlos olivine analyzed by us (Table 3) and the observations of Boland and Duba (1986) that, in San Carlos olivine, similarly reducing conditions caused the precipitation of Ni-Fe alloy. It is possible that our orthopyroxene behaved similarly, but energy and wavelength-dispersive analyses did not show a convincing increase in Ni X-rays emitted from the vicinities of individual surface blebs (located with backscattered electron images). More important is the observation that new impedance arcs appeared when the orthopyroxene crystal was first subjected to reducing conditions. We are confident that the new arcs are related to the appearance of the microstructure.
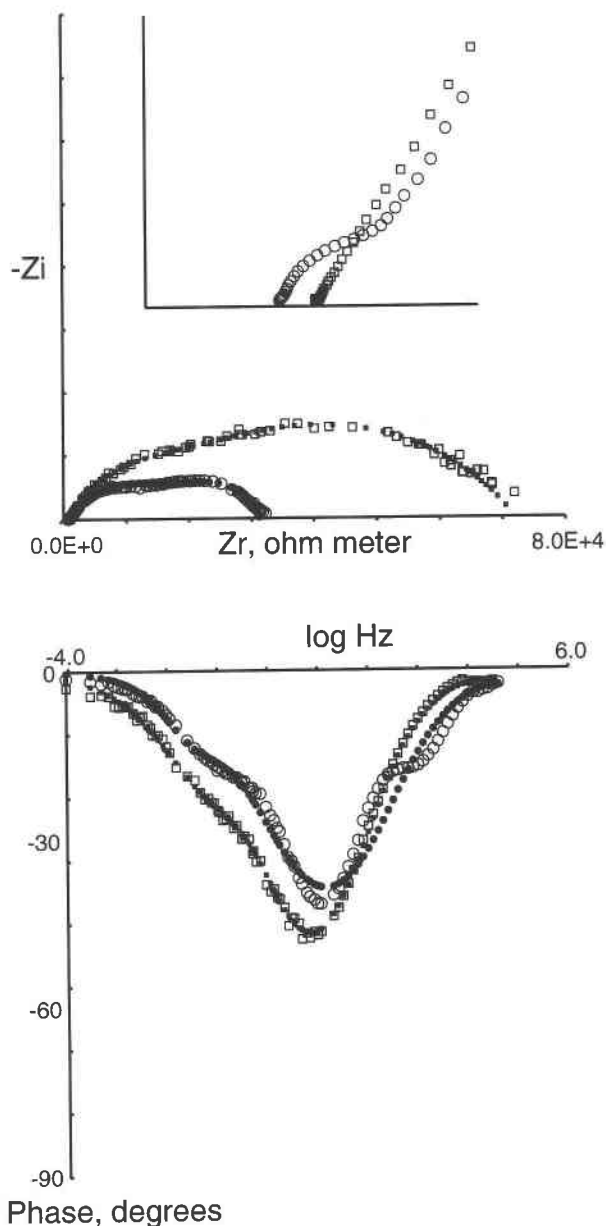

Fig. 8. Orthopyroxene MF1b, 1050 °C. Squares, log $f_{O_2} = -11$, at 342 h. Circles, log $f_{O_2} = -14$, at 510 h. Furnace f_{O_2} changed at 363 h. (top) Complex-plane plot; inset shows that a new, high-frequency arc developed after exposure to reducing conditions. (bottom) Phase-frequency plot. The spectrum at lower f_{O_2} shows additional relaxations at 1 and 10^3 Hz. Open squares are measured impedances; filled squares are calculated from the model.

Olivine single crystals

Olivine single crystals provided our best evidence that the low-frequency arc is due to sample-electrode interaction. At 1000–1150 °C, all spectra of the thin SC2c plate consisted of a semicircular high-frequency arc and a depressed low-frequency arc, 5–10 times as wide as the high-frequency arc. This depressed arc was composite. Visual inspection and CNLS fitting showed that it in-
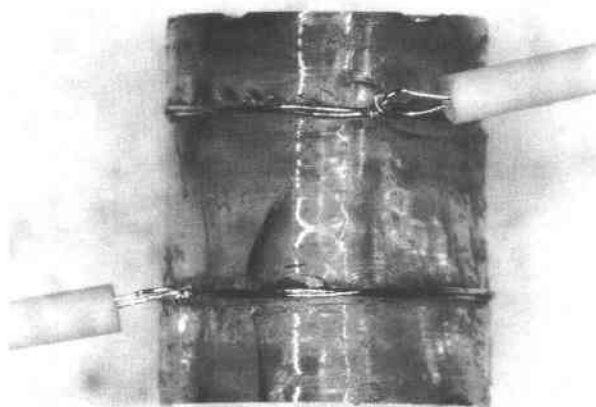
Fig. 9.   Olivine single-crystal Synfo₈₅ equipped for simultaneous two- and four-electrode measurements. Each inner voltage electrode consists of two turns of 0.0001-m Pt wire. When positioned in the sample cell, Ir plates are in contact with the ends of the olivine cylinder and serve as the outer or current-voltage electrodes. Crystal length = 0.00697 m; outer diameter = 0.00587 m.

creased in size as temperature decreased. The observation that at 1000–1150 °C the arc closed suggests some electronic conduction across the sample-electrode interface; if all charge carriers had been blocked, we would have seen a CPE response at low frequency. (Schock et al., 1989, concluded that in the **c** direction, conduction was dominantly by movement of Mg vacancies.) At 800–900 °C, we could not distinguish the form of the low-frequency feature (ZARC with a very large resistance or CPE) because we could not make measurements at sufficiently low frequencies. It is conceivable that there was no electronic conduction across the interface at ≤900 °C.

Olivine single-crystal Synfo₈₅ was sufficiently long (0.00697 m) that it could be prepared for simultaneous two- and four-electrode measurements. Two narrow, shallow grooves, girdling the circumference, held two turns each of 0.0001-m Pt wire (Fig. 9) that served as the inner voltage electrodes. The ends of the sample received unusually thick coats of evaporated Pt. The facing surfaces of the Ir plates were painted with a slurry of Ir black and glycerine, then dried with a heat gun so that the slurry could not smear or flow along the fracture, forming a low-resistance electrical path between the end of the sample and an inner electrode. The two-electrode spectra of this 0.007-m crystal were similar to those of the thin plates described above in exhibiting a semicircular high-frequency arc and a depressed low-frequency arc. The low-frequency arc was small, compared with the high-frequency arc, in the initial spectra, but over a period of several days it increased and became approximately equal to the high-frequency arc (Fig. 10). We attribute the initial small size of the low-frequency arc to the thick coating of vaporized Pt, which we presume made excellent initial contact with the sample. After all measurements were completed, scanning electron microscopy revealed
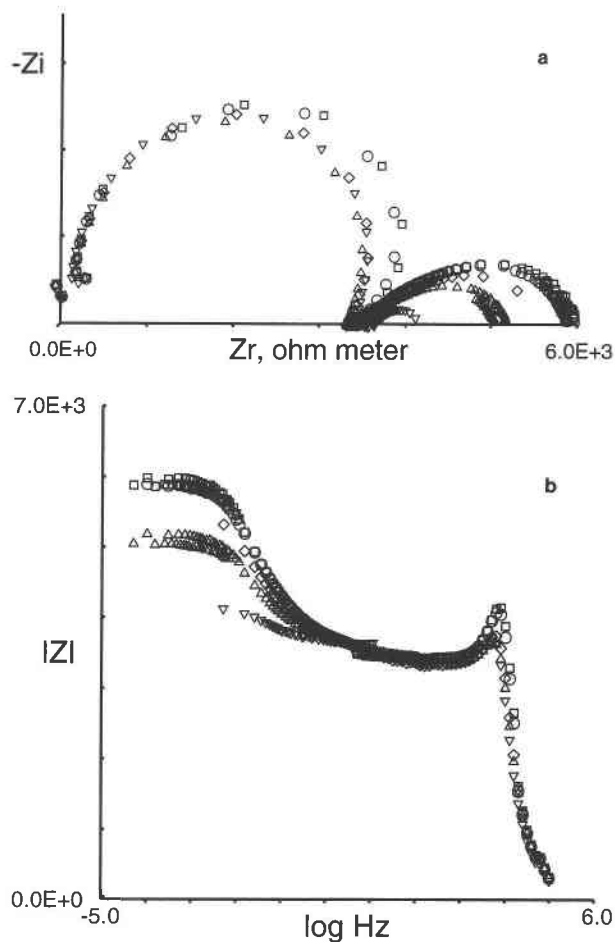

Fig. 10.   Two-electrode impedance spectra of Synfo₈₅. When first heated (at 1050 °C and log f_{O_2} = −13.0), the impedance of the low-frequency arc (**a**) or plateau (**b**) progressively increased with time, whereas the high-frequency arc or plateau was relatively stable. Spectra represented by inverted triangles, upright triangles, diamonds, circles, and squares were initiated 3, 31, 120, 176, and 200 h, respectively, after furnace conditions were first reached. The overlap of points within the second and fifth spectra occurs because measurement of 20 points in the range 0.05–5.65 mHz is completed before measurement of an additional 20 points in the range 0.10–11.30 mHz begins (see Table 1).

that the Pt film had redistributed itself in the form of minute, discontinuous blebs and that electrical contact between this discontinuous film and the Ir electrodes was made through larger, irregularly shaped blebs of Ir.

In the complex plane, high-frequency arcs in spectra of Synfo₈₅ appear to have centers above the real axis; in the Bode-magnitude plots, there is an impedance maximum of high frequency (Fig. 10). These features can be caused by inductance in the measurement leads and instrumentation, or by nonlinear sample response. We observed inductive features only when measuring long samples. We hypothesized that when the thin samples were measured, the closely-spaced Ir electrode plates contributed significant capacitance to mask inductance in the system. When
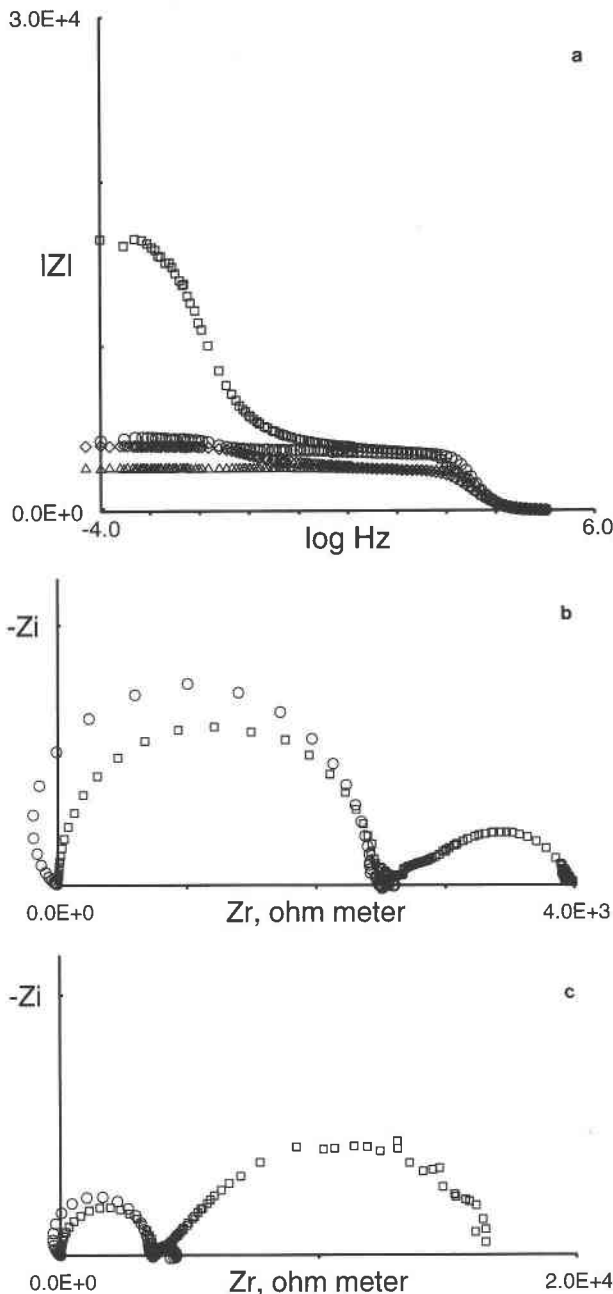
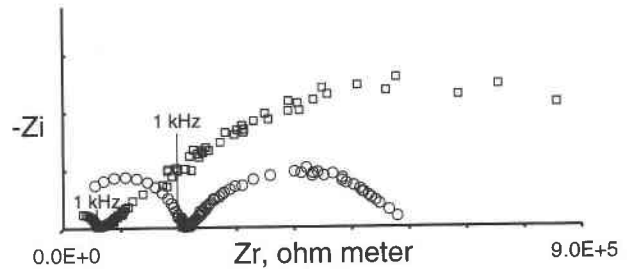Fig. 12. Comparison of single-crystal DK7a (circles) and polycrystal DK7sp2 (squares), both at 1000 °C and log f_{O_2} = −13.0. The single-crystal spectrum has subequal arcs, whereas the low-frequency arc dominates the spectrum of the polycrystal. There is no distinct arc attributable to grain boundaries in the polycrystals.

Fig. 11. Comparison of two- and four-electrode spectra at log f_{O_2} = −13.0. (a) Two-electrode spectra (squares, 1000 °C; circles, 1100 °C) show pronounced low-frequency response whereas four-electrode spectra (diamonds, triangles) do not. The impedance maxima, seen at 10 kHz in Fig. 10b, were suppressed by adding capacitance to the measured circuit (see text). Complex plane plots of the same spectra (b, 1100 °C; c, 1000 °C) clearly show that the true four-electrode method suppresses the low-frequency arc that is attributed to sample-electrode interaction.

the electrodes were moved apart, the cell capacitance decreased, and inductive effects were resolved. A small capacitor (40–176 pF) placed in parallel with the cell eliminated the high-frequency impedance maximum in the

Bode plot (Fig. 11) but did not alter the values of the impedance, thereby eliminating the interference and confirming our hypothesis.

The purpose of the true four-electrode method is to avoid measuring the potential due to the space-charge polarization that accumulates at interfaces between unlike materials and that increases with the flow of current across the interface. If the low-frequency arc is caused by the sample-electrode interface (rather than by the bulk sample), measurement of the voltage drop across the interior electrodes using an electromer (drawing negligible current) should eliminate the low-frequency arc seen in two-electrode measurements. Our observations confirm the hypothesis: in contrast with the two-electrode spectra, a four-electrode spectrum has only one large arc, with the same width as the high-frequency arc in the two-electrode spectra (Fig. 11). We conclude that the low-frequency arc observed in all spectra of pyroxene and olivine single crystals is due to electrode-sample interaction and is not a property of the bulk sample. Further, the fact that the initial low-frequency arc was small and that, with one exception (SC2c at low temperature), low-frequency arcs approached the real axis of complex-plane plots at the lowest frequencies measured suggests that the initial (and continuous) metallic coat was not blocking the dominant charge carriers, leading us to propose that the dominant charge carriers are electrons (or electron holes).

Pyroxene polycrystals

We expected that sintered aggregates of DK7 would show a distinct new resonance due to grain boundaries; that was not the case (Fig. 12). However, spectra of diopside aggregate differed from spectra of the DK7 single crystal in two respects: in the polycrystal, the low-frequency arc was much larger than the high-frequency arc and at lowest frequencies never reached the Z_r axis. Furthermore, even when the low-frequency arc appeared semicircular and almost closed, CNLS fits were improved when the arc was fitted to two ZARCs. In some other cases, the arc had a curvature at low frequency, suggesting that it might reach the Z_r axis at lower frequencies than
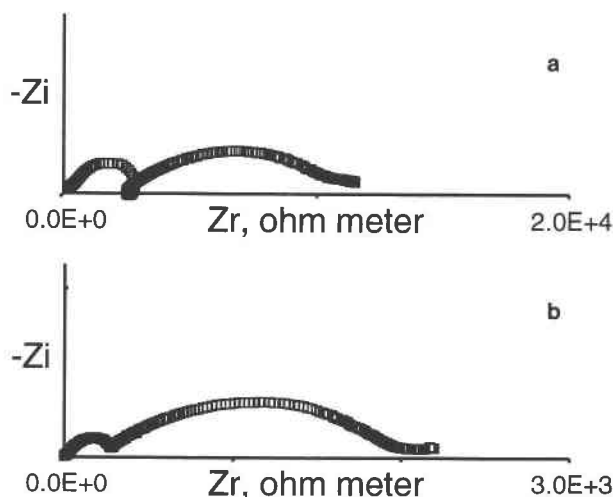
Fig. 13. Comparison of two- and true four-electrode impedance spectra of clinopyroxenite at 750 °C, 1 bar, and log f_{O_2} = −16.0. (a) The two-electrode spectrum consists of a depressed low-frequency arc (sample-electrode interaction), and a composite high-frequency arc. The major portion of the high-frequency arc is probably due to grain boundaries; the small, incomplete, overlapping highest frequency arc is due to grain interiors. (b) The four-electrode spectrum of the sample interior (grain interiors and grain boundaries). The width of the four-electrode arc is comparable with the grain-interior and grain-boundary arcs in the two-electrode high-frequency arc, a. The low-frequency tail at Z_r > 2 kΩ is probably an artifact of the low-frequency response of the impedance analyzer, not a sample response.
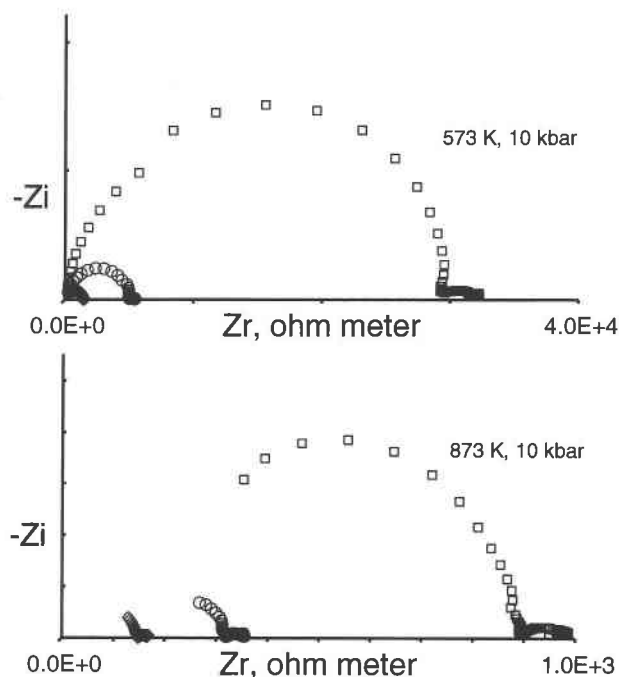

Fig. 14. Representative impedance spectra of clinopyroxenite at 10 kbar and 100 K increments, 300–800 K. The high-frequency semicircular arc dominates the spectrum in all cases.

those available with our instrumentation. In yet other cases, with decreasing frequency, the curvature gave way to a straight trend (Z_i/Z_r tended to assume a constant value). This linear trend in the complex plane could be modeled as a CPE element or a ZARC with a very large resistance. In all cases, introduction of a third element improved the CNLS fitting parameters and the visually perceived match of measured and modeled spectra. Had we not found three elements necessary to obtain good fits to the pyroxene single-crystal spectra, we might have concluded that the middle arc was the response to the presence of grain boundaries. Instead, we suggest that the expected response exhibited by grain boundaries in DK7 polycrystal is indistinguishable from the response due to the sample-electrode interfaces.

Clinopyroxenite at 1 bar

Some measurements of CPxnt were hampered by a maximum in the impedance magnitude (or a looping back in the complex plane) at 10^4–10^5 Hz. Our conclusions are based on spectra that did not show an appreciable maximum or loop, one set of which is shown in Figure 13. Two-electrode measurements consist of a depressed low-frequency arc that is distinct from a smaller arc that lies at higher frequency (Fig. 13a). With increasing frequency, this smaller arc does not trend toward the Z_r axis and the origin of the complex plane; rather, it overlaps a yet

smaller arc at highest frequency. The most obvious interpretation is that, with decreasing frequency, the three arcs represent grain-interior, grain-boundary, and sample-electrode relaxations. The four-electrode spectra of the interior of the clinopyroxenite (Fig. 13b) consist of a small, semicircular, high-frequency arc that is similar to the grain-interior arcs of single crystals and a relatively large, depressed, low-frequency arc that is flatter than the middle arc of the two-electrode spectrum and similar to the sample-electrode arcs. The entire four-electrode spectrum falls within the high-frequency composite arc of the two-electrode spectrum. We are confident that the highest-frequency arcs in both spectra are due to grain interiors and tentatively assign the four-electrode, low-frequency arc to grain boundaries.

Clinopyroxenite at high pressure

Representative spectra, 300–800 °C, are shown in Figure 14. Each spectrum consists of a semicircular high-frequency arc and a much smaller, depressed, low-frequency arc. As before, we attribute the high-frequency semicircular arc to grain-interior conduction. The low-frequency arc is not well resolved; we presume that it contains the sample-electrode and grain-boundary responses. It is reasonable to interpret the small size of the depressed arc as caused by the increase in pressure, improving the contact between the electrodes and the clinopyroxenite (in a manner perhaps similar to the thick Pt film on the synthetic olivine) and closing grain boundaries, thereby improving electrical transport between grains.
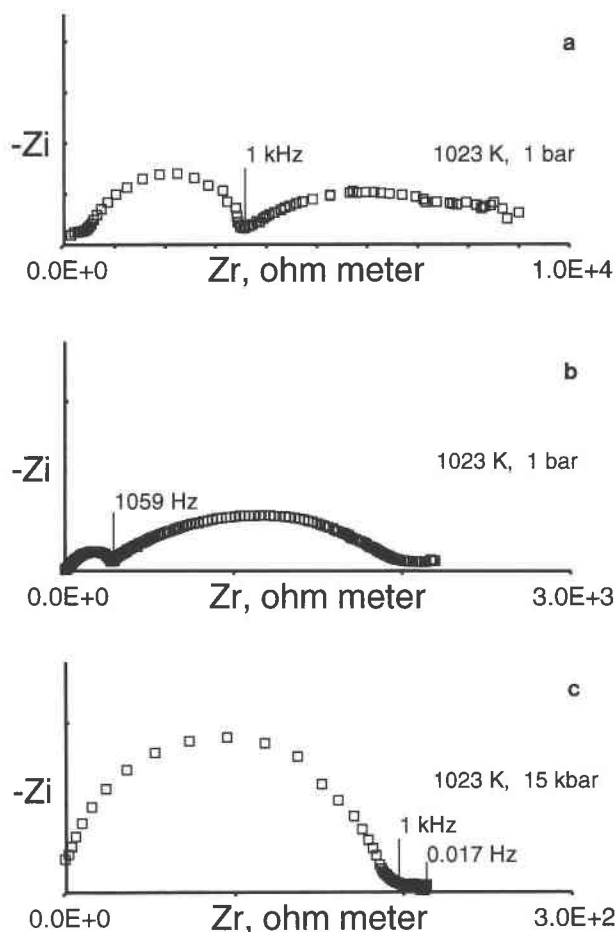
Fig. 15. Comparison of clinopyroxenite spectra taken at 750 °C, shown in the complex plane. (a) At 1 bar, with two electrodes, there are three distinct relaxations due to grain interiors (small, incomplete high-frequency arc, near origin), grain-boundaries, and sample-electrode interactions (large flattened arc). (b) At 1 bar, with four electrodes, the spectrum obtained from the inner electrodes shows two relaxations due to grain interiors and grain boundaries. The sample-electrode response is not significant. (c) At 15 kbar, the large, semicircular, grain-interior arc dominates the spectrum; the arc caused by grain-boundary and sample-electrode interactions is small.

Spectra of clinopyroxenite, acquired at 1 bar and 15 kbar, are compared in Figure 15. Compared with the 1-bar, outer (two-) electrode technique, the 1-bar, inner (four-) electrode technique suppresses the low-frequency, sample-electrode interaction. Measurement at 15 kbar suppresses both sample-electrode and grain-boundary responses. The grain interior arc can be seen in all three spectra; at 1 bar it appears as a relatively minor arc, but at 15 kbar it dominates the spectrum. The effect of increasing pressure from 1 to 10–20 kbar is consistent over the temperature ranges of measurement (Fig. 16). Results of CNLS fitting show that pressure has little effect on the grain-interior impedances. But it is clear that increasing pressure markedly decreases the low-frequency responses.
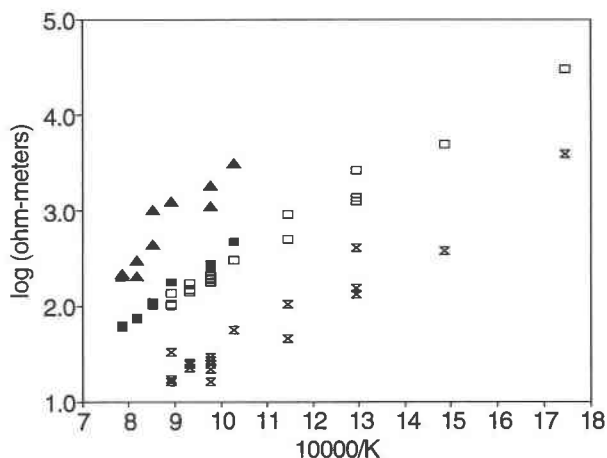

Fig. 16. Results of CNLS fitting of clinopyroxenite impedance spectra measured at 1 bar (solid symbols) and at 10–20 kbar (open symbols). Squares designate the high-frequency arc (grain interior); triangles and diamonds designate the low-frequency arcs. Over the temperature range common to both pressures, the resistance of the grain interiors at low pressure (four-electrode technique) and high pressure are similar. In contrast, increasing pressure markedly decreases the resistance of the low-frequency arcs.

SUMMARY OF OBSERVATIONS AND INTERPRETATION

Impedance spectra of natural silicate minerals and rocks usually contain more than two relaxations in the frequency range 10^{-4}–10^5 Hz. Commonly, single crystals and some aggregates show a grain-interior arc at high frequencies and a complex, low-frequency arc related to sample-electrode interactions. The grain-interior arc is always semicircular. The sample-electrode arc (and its resolvable overlapping components) are always depressed arcs. With difficulty, we have been able to distinguish clearly an arc that in frequency lies between those due to grain interiors and sample-electrode interactions. We assign this arc to grain boundaries. But in many cases, the grain-boundary response is not distinct.

At 1 bar, the resistance associated with grain interiors is small relative to that of the other responses. Thus, at low frequencies (1 mHz) and laboratory pressures, the principal barriers to conduction are due to sample-electrode interactions at low frequency and grain boundaries at intermediate frequency. Increased pressure (10 kbar) so decreases the resistance associated with the sample-electrode interfaces and grain boundaries that the dominant resistance is due to the grain interiors.

The nature and evolution of the electrodes used to make contact with the sample is a critical problem. Pt films are not stable, particularly at high temperature. Heterogeneous sample-electrode interfaces, such as those encountered at 1 bar and particularly at high temperature, can cause much of the measured impedance at low frequency. A slurry of Ir black, suspended in a vehicle that evaporates or decomposes on heating, offers much promise as
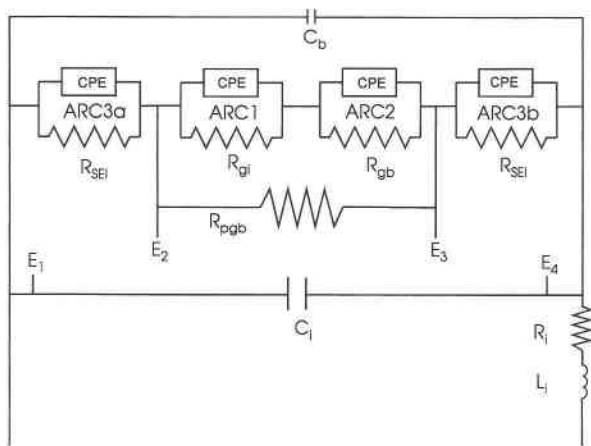
Fig. 17. Schematic of generic model network. SEI is sample-electrode interface; gi is grain interior; gb is grain boundary (if sample is polycrystalline). R_{pgb} is the resistance to the flow of current along a path that follows grain boundaries (and does not cross into grain interiors). C_i, R_i, and L_i are capacitance, resistance, and inductance associated with measurement instrumentation and leads (here shown only for the outer electrodes). E_1–E_4 are leads from electrodes to impedance-measurement instrumentation (see Fig. 4).

a high-temperature electrode; if the vehicle dries soon after application, so much the better.

Most arcs caused by sample-electrode interactions approach the real axis with decreasing frequency, indicating the existence of a path by which charge carriers conduct across the interface (the resistance is not infinite). Because our metallic electrodes, ultimately the Ir plates, are blocking to all ions and vacancies present in the silicates, there must be significant electronic conduction across the sample-electrode interface. Were this charge to be totally transported by charged ions, there would be no flow of charged species across the interface, the resistance would be infinite, and the low-frequency arcs would not close. Rather, the spectra would terminate with a constant-phase element, as observed for lithium silicates and aluminosilicates by Raistrick et al. (1976) and for sandstones partially saturated with H_2O vapor (Knight, 1983).

IMPLICATIONS FOR GEOPHYSICAL INTERPRETATION

We have shown that most samples show three (or more) relaxations, separated in frequency. Most previous measurements, made for the purpose of obtaining electrical conductivities of rocks, have been made at a single frequency. Without an impedance spectrum, we must make assumptions about the nature of the response (or sum of responses) that was measured. Finally, increasing pressure in the laboratory changes the relative importance of these responses for conduction; similar changes can be expected within the Earth's crust. These observations lead to two questions. (1) Of what value are existing laboratory measurements for interpreting low-frequency con-

ductivities of the Earth's interior? (2) How might relevant future measurements be most easily made?

(1) Because many monofrequency measurements of dry rocks in the laboratory have been made at a total pressure of 1 bar, we indicated data taken at or close to 1 kHz in our Figures 12 and 15; some of the other figures are plotted as a function of frequency. Two-electrode impedance-conductivity measurements of rock at 1 kHz and 1 bar are unlikely to distinguish the grain-interior and grain-boundary responses, and the grain-boundary response may be the dominant resistance term. Although the grain-interior conduction is relatively insensitive to pressure, the resistance that the grain boundaries offer to conduction drops dramatically with increasing pressure. Thus, we predict that the conventional two-electrode technique used at 1 kHz and 1 bar will overestimate the resistance of rocks at high pressures within the crust. Figures 13 and 15 suggest that it is possible to underestimate the conductivity by a factor of 5–10.

(2) Although the conductivity of pure forsterite and diopside are sensitive to changes in f_{O_2}, this sensitivity decreases with the substitution of Fe^{2+}, Fe^{3+}, Al, and the common minor elements found in rock-forming minerals. In the future we will report that the conductivity of Kangan augite and CPxnt clinopyroxenite are relatively insensitive to f_{O_2}. Perhaps the most geologically relevant data can be obtained using a piston-cylinder apparatus and controlled temperature and pressure, allowing the sample to buffer itself with respect to f_{O_2}. At these conditions, the grain boundaries will be tight, as in the interior of the crust. A sufficient number of measurements to define the grain-interior arc can be made in a few minutes, and the small grain-boundary response can be estimated if necessary. The rate limiting factor probably is sample equilibration.

IMPLICATIONS FOR MINERAL PHYSICS

The frequency at which the grain-interior arc (or any other arc) touches the real axis varies with temperature because the resistance varies strongly with temperature (and the dielectric constant does not). Therefore, when determining how conductivity varies with temperature, it is not sufficient to show that conductivity is independent of frequency at only one temerature; it would be better to demonstrate constancy throughout each temperature range in question. We suspect that reported log-conductivity slopes and thermal activation energies contain a slight systematic error.

Point-defect mechanisms proposed to explain the electrical conductivity of a material must be consistent with the low-frequency sample-electrode response. A low-frequency arc indicates the presence of a path by which charge flows across the interface and into the electrodes. If the electrodes are an inert metal such as Ir or Pt, electronic species must be present at the interface. The low-frequency response caused by electrodes that are blocking to the charge carriers at the interface must be a CPE response.

GENERIC MODEL

Our results on dry minerals and rocks, coupled with the results of those earlier investigators who measured wet rocks, lead to an understanding of the factors that affect impedance spectra and thus to a generic model (Fig. 17) for interpreting impedance spectra. This model also helps us understand conduction through minerals, and rocks, and synthetic aggregates such as concrete. The model has five parts, but not all are likely to be seen in a single spectrum.

(1) Grain interiors have a grain-interior resistance, R_{gi}, shown in ARC1. The empty cell has a capacitance C_{ec} ($C_{ec} = 0.8$ pF for 0.01-m Ir electrode separation). When a sample having the bulk dielectric constant K_b is placed between the Ir electrodes, the capacitance increases by $C_s = (K_b - 1)C_{ec}$. This bulk geometric capacitance, $C_b = K_b C_{ec}$, is relatively small and appears as the capacitance seen in ARC1 of the model. (Any instrumental capacitance, C_i, is seen as an addition to $C_s + C_{ec}$.) ARC1 is an almost ideal, semicircular arc (response of a ZARC having $\phi \sim 1$) and is seen at high frequency (a consequence of capacitance of the order of 10–100 pF). We hypothesized that a bimineralic sample with two distinct values of R_{gi} (or two distinct grain-interior time constants) should show two overlapping high-frequency impedance arcs, but we have not yet observed such a feature.

(2) Flow across grain boundaries (if present) should cause a second arc, ARC2. These boundaries juxtapose unlike materials (grain interior and grain-boundary medium) so the capacitance is likely to be large, particularly if there are many boundaries, or water is present in the grain boundaries. The grain-boundary resistance is expected to be high in dry rock at low pressure, intermediate in dry or wet rock at high pressure, and low in wet rock at low pressure. Heterogeneity of grain-boundary width, composition, and spacing should lead to a depressed ZARC ($\phi < 1$).

(3) Flow through the grain-boundary medium, R_{pgb}. This path bypasses (short circuits) elements 1 and 2, above. If the conduction along the grain-boundary medium is a minor component of total conduction, the effect on the impedance spectrum is to shrink the largest parallel arc, making recognition difficult. If conduction along grain boundaries is the dominant path, as in wet rocks having high porosity and permeability, ARC2 and ARC1 may not be evident.

(4) Sample-electrode interactions occur at each end of the sample and form one response or overlapping low-frequency responses. Because the sample and electrodes are different materials, there always is a capacitive term associated with the interfaces. If the electrodes are totally blocking (to the charge carriers in the sample) the response is that of a CPE element; if they are nearly totally blocking, the response is a broad ZARC that appears as a CPE; if they are partially blocking, the response is a ZARC; if they are more conductive than the sample, the response is a ZARC that will probably not be seen.

(5) The impedance instrumentation and leads are associated with values of series R_i (negligibly small), parallel R_i (much larger than the resistance of the sample and cell and therefore neither detected nor shown), parallel C_i (<3 pF, seen as an addition to $C_{ec} + C_s$), and series L_i (not detected).

A note of caution is necessary when normalizing the sample response to that of a cube, 1 m on edge, by multiplying the spectrum's impedance values by a volume factor calculated from the area and length of a sample. Instrumental components included in the spectrum should not be normalized, and the component due to the sample-electrode interface should be normalized only with respect to area. The effect of volume normalization is to magnify the instrumental and interfacial signatures.

REFERENCES CITED

Abelard, P., and Baumard, J.F. (1980) Electric and dielectric properties of forsterite between 400 and 900 °C. Physics of the Earth and Planetary Interiors, 23, 98–102.

Baedecker, P.A., and McKown, D.M. (1987) Instrumental neutron activation analysis of geochemical samples. In P.A. Baedecker, Ed., Methods for geochemical analysis. U.S. Geological Survey Bulletin 1770, H1–H14.

Boland, J.N., and Duba, A.G. (1986) An electron microscope study of the stability field and degree of nonstoichiometry in olivine. Journal of Geophysical Research, 91, 4711–4722.

Boukamp, B.A. (1984) A microcomputer based system for frequency dependent impedance/admittance measurements. Solid State Ionics, 11, 339–346.

Cermak, V., and Lastovickova, M. (1987) Temperature profiles in the Earth of importance to deep electrical conductivity models. Pageoph, 125, 255–284.

Chu, S.H., and Seitz, M.A. (1978) The ac electrical behavior of polycrystalline ZrO$_2$-CaO. Journal of Solid State Chemistry, 23, 297–314.

Constable, S., and Duba, A. (1990) Electrical conductivity of olivine, a dunite, and the mantle. Journal of Geophysical Research, 95, 6967–6978.

Duba, A. (1972) Electrical conductivity of olivine. Journal of Geophysical Research, 77, 2483–2495.

Duba, A., Heard, H.C., and Schock, R.N. (1974) Electrical conductivity of olivine at high pressure and under controlled oxygen fugacity. Journal of Geophysical Research, 79, 1667–1673.

Gerhardt, R., and Nowick, A.S. (1986) Grain-boundary effect in ceria doped with trivalent cations: I. Electrical measurements. Journal of the American Ceramic Society, 69, 641–646.

Hanson, D.R., Young, M., and Ryerson, F.J. (1991) Growth and characterization of synthetic iron-bearing olivine. Physics and Chemistry of Minerals, 18, 53–63.

Hinze, E., Will, G., and Cemic, L. (1981) Electrical conductivity measurements on synthetic olivines and on olivine, enstatite and diopside from Dreiser Weiher, Eifel (Germany) under defined thermodynamic activities as a function of temperature and pressure. Physics of the Earth and Planetary Interiors, 25, 245–254.

Hodge, I.M., Ingram, M.D., and West, A.R. (1976) Impedance and modulus spectroscopy of polycrystalline solid electrolytes. Journal of Electroanalytical Chemistry, 74, 125–143.

Huebner, J. S. (1987) Use of gas mixtures at low pressure to specify oxygen and other fugacities of furnace atmospheres. In G.C. Ulmer and H.L. Barnes, Eds., Hydrothermal experimental techniques, p. 20–60. Wiley, New York.

Huebner, J. S., and Voigt, D.E. (1988) Electrical conductivity of diopside: Evidence for oxygen vacancies. American Mineralogist, 73, 1235–1254.

Huebner, J. S., Duba, A., and Wiggins, L.B. (1979) Electrical conductivity of pyroxene which contains trivalent cations: Laboratory measurements and the lunar temperature profile. Journal of Geophysical Research, 84, 4652–4656.

Hurt, R.L., and Macdonald, J.R. (1986) Distributed circuit elements in impedance spectroscopy: A unified treatment of conductive and dielectric systems. Solid State Ionics, 20, 111–124.

Kirby, S.H., and Christie, J.M. (1977) Mechanical twinning in diopside Ca(Mg,Fe)Si₂O₆. Structural mechanism and associated crystal defects. Physics and Chemistry of Minerals, 1, 137–163.

Kleitz, M., Bernard, H., Fernandez, E., and Schouler, E. (1981) Impedance spectroscopy and electrical resistance measurements on stabilized zirconia. In A.H. Heuer and L.W. Hobbs, Eds., Advances in ceramics, vol. 3, p. 310–336. American Ceramic Society, Columbis, Ohio.

Knight, R.J. (1983) The use of complex plane plots in studying the electrical response of rocks. Journal of Geomagnetism and Geoelectricity, 35, 767–776.

Knight, R.J., Nur, A., and Raistrick, I.D. (1985) Modelling the electrical response of sandstones with an equivalent circuit. Transactions of the Society of Professional Well Log Analysts, 26th Annual Logging Symposium, M1–M15.

Lastovickova, M. (1987) Electrical conductivity of some minerals at high temperature and for extended times. Physics of the Earth and Planetary Interiors, 45, 204–208.

——— (1991) A review of laboratory measurements of the electrical conductivity of rocks and minerals. Physics of the Earth and Planetary Interiors, 66, 1–11.

Lee, C.D., Vine, F.J., and Ross, R.G. (1983) Electrical conductivity models for the continental crust based on laboratory measurements on high-grade metamorphic rocks. Geophysical Journal of the Royal Astronomical Society, 72, 353–371.

Lockner, D.A., and Byerlee, J.D. (1985) Complex resistivity measurements of confined rock. Journal of Geophysical Research, 90, 7837–7847.

Macdonald, J.R. (1976) Interpretation of AC impedance measurements in solids. In G.D. Mahan and W.L. Roth, Eds., Proceedings of the conference on superionic conductors—chemistry, physics, and applications, p. 81–97. Plenum, New York.

———, Ed. (1987) Impedance spectroscopy, emphasizing solid materials and systems, 346 p. Wiley, New York.

Macdonald, J.R., and Potter, L.D., Jr. (1987) A flexible procedure for analyzing impedance spectroscopy results: Description and illustrations. Solid State Ionics, 23, 61–79.

Macdonald, J.R., Schoonman, J., and Lehnen, A.P. (1981) Three dimensional perspective plotting and fitting of immittance data. Solid State Ionics, 5, 137–140.

——— (1982) The applicability and power of complex nonlinear least squares for the analysis of impedance and admittance data. Journal of Electroanalytical Chemistry, 131, 77–95.

Matsui, N. (1986) Equivalent circuit analysis of high temperature solid electrolyte. Solid State Ionics, 18/19, 888–891.

Olhoeft, G.R. (1979) Electrical properties. In G.R. Hunt, G.R. Johnson, G.R. Olhoeft, D.E. Watson, and K. Watson, Eds., Initial report of the petrophysics laboratory. U.S. Geological Survey Circular 789, p. 1–26.

——— (1985) Low-frequency electrical properties. Geophysics, 50, 2492–2503.

Raistrick, I.D., Ho, C., and Huggins, R.A. (1976) Ionic conductivity of some lithium silicates and aluminosilicates. Journal of the Electrochemical Society, 123, 1469–1476.

Roberts, J.J., and Tyburczy, J.A. (1991) Frequency dependent electrical properties of polycrystalline olivine compacts. Journal of Geophysical Research, 96, 16205–16222.

——— (1993) Impedance spectroscopy of single and polycrystalline olivine: Evidence for grain boundary transport. Physics and Chemistry of Minerals, 20, 19–26.

Sato, H., and Ida, Y. (1984) Low frequency electrical impedance of partially molten gabbro: The effect of melt geometry on electrical properties. Tectonophysics, 107, 105–134.

Schock, R.N., Duba, A.G., and Shankland, T.J. (1989) Electrical conduction in olivine. Journal of Geophysical Research, 94, 5829–5839.

Shankland, T.J., and Duba, A.G. (1990) Standard electrical conductivity of isotropic, homogenous olivine in the temperature range 1200°–1500 °C. Geophysical Journal International, 103, 25–31.

Skogby, H., Bell, D.R., and Rossman, G.R. (1990) Hydroxide in pyroxene: Variations in the natural environment. American Mineralogist, 75, 764–774.

Wanamaker, B.J., and Duba, A.G. (1993) Electrical conductivity of San Carlos olivine along [100] under oxygen- and pyroxene-buffered conditions and implications for defect equilibria. Journal of Geophysical Research, 98, 489–500.

Wellstead, P.E. (1983a) Frequency response analysis. Schlumberger Technical Report 010/83, 16 p.

——— (1983b) Frequency domain techniques for conditioning monitoring of rotating machinery. Schlumberger Technical Report 011/83, 17 p.